International Journal of Obesity (2014), 1–8

www.nature.com/ijo

ORIGINAL ARTICLE

Genetic ablation of macrohistone H2A1 leads to increased leanness, glucose tolerance and energy expenditure in mice fed a high-fat diet

F Sheedfar[1], M Vermeer[1], V Pazienza[2], J Villarroya[3,4], F Rappa[5], F Cappello[5,6], G Mazzoccoli[7], F Villarroya[3], H van der Molen[1], MH Hofker[1,9], DP Koonen[1,9] and M Vinciguerra[2,6,8,9]

BACKGROUND/OBJECTIVES: In the context of obesity, epigenetic mechanisms regulate cell-specific chromatin plasticity, perpetuating gene expression responses to nutrient excess. MacroH2A1, a variant of histone H2A, emerged as a key chromatin regulator sensing small nutrients during cell proliferation and differentiation. Mice genetically ablated for macroH2A1 (knockout (KO)) do not show overt phenotypes under a standard diet. Our objective was to analyse the *in vivo* role of macroH2A1 in response to nutritional excess.

METHODS: Twelve-week-old whole-body macroH2A1 KO male mice were given a high-fat diet (60% energy from lard) for 12 weeks until being killed, and examined for glucose and insulin tolerance, and for body fat composition. Energy expenditure was assessed using metabolic cages and by measuring the expression levels of genes involved in thermogenesis in the brown adipose tissue (BAT) or in adipogenesis in the visceral adipose tissue (VAT).

RESULTS: Under a chow diet, macroH2A1 KO mice did not differ from their wild-type (WT) littermates for body weight, and for sensitivity to glucose or insulin. However, KO mice displayed decreased heat production ($P < 0.05$), and enhanced total activity during the night ($P < 0.01$). These activities related to protection against diet-induced obesity in KO mice, which displayed decreased body weight owing to a specific decrease in fat mass ($P < 0.05$), increased tolerance to glucose ($P < 0.05$), and enhanced total activity during the day ($P < 0.05$), compared with WT mice. KO mice displayed increased expression of thermogenic genes (*Ucp1*, $P < 0.05$; *Glut4*, $P < 0.05$; *Cox4*, $P < 0.01$) in BAT and a decreased expression of adipogenic genes (*Pparγ*, $P < 0.05$; *Fabp4*, $P < 0.05$; *Glut4*, $P < 0.05$) in VAT compared with WT mice, indicative of augmented energy expenditure.

CONCLUSIONS: Genetic eviction of macroH2A1 confers protection against diet-induced obesity and metabolic derangements in mice. Inhibition of macroH2A1 might be a helpful strategy for epigenetic therapy of obesity.

International Journal of Obesity advance online publication, 17 June 2014; doi:10.1038/ijo.2014.91

INTRODUCTION

The current pandemic in obesity/metabolic syndrome is a risk factor for many types of diseases, including cardiovascular diseases and cancer.[1,2] Epigenetic mechanisms of nuclear chromatin remodelling, such as DNA methylation, posttranslational modifications of histones and incorporation of histone variants into the chromatin, are increasingly recognized as crucial factors in the pathophysiology of obesity and related complications.[3] In fact, metabolic alterations in peripheral tissues are triggered at the cellular level by changes in gene transcriptional patterns dependent on the degree of nuclear chromatin compaction. The latter is regulated at several levels, allowing transcriptional plasticity:[4] one way is the replacement of canonical histones around which DNA is wrapped (H2A, H2B, H3 and H4) with the incorporation of histone variants. The histone variant of H2A, known as macroH2A1, is believed to act as a strong transcriptional modulator that can either repress transcription[5,6] or activate it in response to as yet undefined nutrients or growth signals.[7] The transcriptional activity of macroH2A1 has come to take a centre stage in the plasticity of stem cell differentiation and in the pathogenesis of many cancer types.[8–11] MacroH2A1 is composed of a domain displaying 66% homology with histone H2A, and a domain called macro that is conserved in multiple functionally unrelated proteins throughout the animal kingdom and that can bind *in vitro* with tight affinity ADP-ribose-like metabolites produced by NAD+-dependent histone deacetylase sirtuins or by polyADP-ribose polymerase enzymes.[12,13] This binding represents a direct molecular interaction between intermediate metabolism and the chromatin, whereby a metabolite can impinge on and tweak gene expression *in vitro*.[14–17]

[1]Department of Pediatrics, Section Molecular Genetics, University of Groningen, University Medical Center Groningen (UMCG), Groningen, The Netherlands; [2]Gastroenterology Unit, Department of Medical Sciences, IRCCS 'Casa Sollievo della Sofferenza' Hospital, San Giovanni Rotondo (FG), Italy; [3]Department of Biochemistry and Molecular Biology, Institute of Biomedicine (IBUB), University of Barcelona, Barcelona, Spain; [4]CIBER Fisiopatologia de la Obesidad y Nutricion, Instituto de Salud Carlos III, Madrid, Spain; [5]Department of Experimental Biomedicine and Clinical Neurosciences, Section of Human Anatomy, University of Palermo, Palermo, Italy; [6]Euro-Mediterranean Institute of Science and Technology (IEMEST), Palermo, Italy; [7]Division of Internal Medicine and Chronobiology Unit, Department of Medical Sciences, IRCCS 'Casa Sollievo della Sofferenza' Hospital, San Giovanni Rotondo (FG), Italy and [8]Institute for Liver and Digestive Health, Division of Medicine, University College London (UCL), UCL Medical School, Royal Free Hospital, London, UK. Correspondence: Dr M Vinciguerra, Institute for Liver and Digestive Health, Division of Medicine, University College London (UCL), UCL Medical School, Royal Free Hospital, Royal Free Campus, Rowland Hill Street, London NW3 2PF, UK.
E-mail: m.vinciguerra@operapadrepio.it
[9]These authors contributed equally to this work.
Received 19 March 2014; revised 6 May 2014; accepted 15 May 2014; accepted article preview online 21 May 2014

Interestingly, in mice models of non-alcoholic fatty liver disease (NAFLD), a disorder that is present in 90% of obese subjects, hepatic content of macroH2A1 is augmented.[18,19] Two mice models, knockout (KO) for macroH2A1, have been reported under a standard diet feeding. In the first model, generated in the pure C57Bl/6J background, developmental changes in macroH2A1-mediated gene regulation were observed.[20,21] In the second model, KO for macroH2A1 in a mixed background led to a variable hepatic lipid accumulation in 50% of the females.[22] Therefore, despite compelling *in vitro* evidence that macroH2A1 modulates gene expression programs involved in cell metabolism, proliferation and differentiation,[9,10] its role at the organism level under nutritional stress conditions, especially during obesity, is not understood. In this study, we challenged macroH2A1 KO mice[20,21] with an obesogenic diet for 12 weeks: we found that genetic ablation of this histone increased leanness, glucose tolerance and energy expenditure, protecting the body against high-fat diet (HFD)-induced obesity.

MATERIALS AND METHODS

Animals and diet

Viable and fertile macroH2A1 KO mice were kindly provided by Prof John Pehrson (University of Pennsylvania, Philadelphia, PA, USA).[20] MacroH2A1 KO mice and their littermates (wild type (WT)) were bred and all procedures were approved by the University of Groningen Ethics Committee for Animal Experiments, which adheres to the principles and guidelines established by the European Convention for the Protection of Laboratory Animals. Mice were housed in a temperature-controlled room under a 12 h light–dark cycle with *ad libitum* access to water and food (2181; RMH-B Arie Blok, Woerden, The Netherlands). At the age of 12–14 weeks, mice were individually housed and fed a HFD composed of 60% kcal fat from lard (D12492; Research Diets, New Brunswick, NJ, USA) for 12 weeks until being killed.

Oral glucose tolerance test and insulin tolerance test

Mice were fasted for 6 h during the daytime, and given a glucose bolus (2 g kg^{-1} of 20% glucose solution) by oral gavage (oral glucose tolerance test (OGTT)) or intraperitoneally (IP) injected with human recombinant insulin (0.5 U kg^{-1} body weight, Actrapid; Novo Nordisk Canada Inc., Mississauga, ON, Canada) (insulin tolerance test (ITT)). Blood was collected from the tail vein and glucose levels were measured with an OneTouch Ultra glucometer (Lifescan Benelux, Beerse, Belgium) before and 15, 30, 60, 90, 120 and 150 min after the gavage/injection.

Dual-energy X-ray absorptiometry scan analysis

Fat and lean mass was determined in HF-fed mice following 11 weeks of dietary intervention using dual-energy X-ray absorptiometry (*P*-DEXA; Norland Stratec Medizintechnik GmbH, Birkenfeld, Germany). Mice were scanned under fed conditions while anaesthetized using isoflurane, and data were analysed according to the manufacturer's instructions.

In vivo metabolic analyses

Groups of 7–8 mice per genotype on HFD were placed individually in indirect calorimetric cages (LabMaster TSE Systems, Bad Homburg, Germany) to enable real time and continuous monitoring of metabolic gas exchange. Following an initial 24-h acclimatization period, mice were monitored every 13 min for 24 h for 4 consecutive days. Heat production, food intake and total activity were analysed. The respiratory exchange ratio (RER) = VCO_2 (volume of CO_2 produced)/VO_2 (volume of O_2 consumed) was used to estimate the percent of carbohydrates and fat contribution to whole-body energy metabolism of mice *in vivo*. Carbohydrate and fat oxidation rates were calculated from VO_2 and VCO_2 according to Peronnet and Massicotte.[23] Faeces were collected and measured by scale.

Analysis of plasma parameters

Insulin was determined in the plasma from 6 h fasted mice using an Enzyme-Linked Immunosorbent Assay Kit (Mercodia Ultrasensitive Mouse Insulin-linked Immunosorbent Assay; Orange Medica, Tilburg, The Netherlands). Triglycerides (TGs) and total cholesterols (TCs) were determined by commercially available kits, according to the manufacturer's instructions (TG: Hitachi; Roche, Woerden, The Netherlands; TC: cholesterol CHOD-PAP; Roche). Roche Percimat Glycerol standard (16658800) and Cholesterol Standard FS (DiaSys Diagnostic Systems Gmbh, Holzheim, Germany) was used as a reference.

Biochemical analyses of Lipids

Total lipids were extracted from the liver according to Bligh and Dyer.[24] Liver and plasma lipid analysis were performed using the available reagent kits (Tri/GB kit Roche, Roche, Mannheim, Germany) based on the manufacturer's protocol.

Immunoblot analyses in mice

The mice were fasted for 6 h and subjected to an IP injection with saline or human recombinant insulin (0.75 U kg^{-1} body weight, Actrapid; Novo Nordisk Canada Inc.) 15 min before being killed. Liver, adipose tissue (interscapular or visceral) and skeletal muscle tissues were rapidly removed and frozen in liquid nitrogen. Powdered tissue was homogenized as described previously.[25] Equal amounts of protein were separated by sodium dodecyl sulfate-polyacrylamide gel electrophoresis, transferred to PVDF membrane (Amersham, Buckinghamshire, UK) and the resulting immune complex was visualized using the Molecular Imager ChemiDoc XRS+System (Bio-Rad, Veenendaal, The Netherlands). Antibodies against phospho- and total AKT were purchased from Cell Signaling (Leiden, The Netherlands). β-Actin (Sigma, Zwijndrecht, The Netherlands) was used as loading control. Densitometry was performed using the Image Lab Software (Bio-Rad).

Histology

Paraffin-embedded sections of the liver or adipose tissue (4 μm) were processed by haematoxylin and eosin for histological evaluation, as described previously.[26,27] Diagnostic classification of NAFLD was performed by applying a semiquantitative scoring system that grouped histological features into broad categories (steatosis, hepatocellular injury, portal inflammation, fibrosis and miscellaneous features).[26] Adipocyte area and perimeter were evaluated using the ImagePro Plus software (Media Cybernetics, Inc., Bethesda, MD, USA).

Gene expression analyses

Quantitative reverse transcriptase PCR (qRT-PCR) experiments were performed as described previously.[28] After homogenization of tissue samples in RLT buffer (Qiagen, Hilden, Germany), RNA was isolated using a column-affinity-based methodology that included on-column DNA digestion (RNeasy; Qiagen). One microgram of RNA was transcribed into cDNA using MultiScribe RT and random hexamer primers (TaqMan Reverse Transcription Reagents; Applied Biosystems, Foster City, CA, USA). For quantitative mRNA expression analysis, TaqMan RT-PCR was performed on the ABI PRISM 7700HT sequence detection system (Applied Biosystems). The TaqMan RT-PCR reactions were performed in a final volume of 25 μl using TaqMan Universal PCR Master Mix, No AmpErase UNG reagent and primer pair probes specific for uncoupling protein-1 (*Ucp1*, Mm00494069), fibroblast growth factor-21 (*Fgf21*, Mm00840165), peroxisome proliferator-activated receptor-γ (*Pparγ*, Mm00440945), glucose transporter-4 (*Glut4*, Slc2a4, Mm00436615), cytochrome *c* oxidase-4 (*Cox4*, Mm00438289), fatty acid-binding protein-4 (*Fabp4*, Mm00445880) and interleukin-6 (*Il-6*, Mm0044619). Controls with no RNA, primers or RT were included in each set of experiments. Each sample was run in duplicate, and the mean value of the duplicate was used to calculate the mRNA levels for the genes of interest. Values were normalized to that of the reference control (*Ppia*, Mm02342430) using the comparative 2 – deltaCT method, following the manufacturer's instructions and represented as fold induction in comparison with WT group.

Rhythmicity of expression of considered genes was verified using CircaDB, a data set of time-course expression experiments from mice and humans deposited as publicly available microarray studies and highlighting circadian gene expression cycles (https://www.bioinf.itmat.upenn.edu/circa).

Statistical analysis

Results are expressed as means ± s.e.m. Comparisons between groups were performed with the parametric Student's *t*-test or the non-parametric Mann–Whitney *U*-test, as appropriate, using GraphPad Prism Software (version 5.00 for Windows, San Diego, CA, USA): a *P*-value $\leqslant 0.05$ was considered significant.

RESULTS

MacroH2A1 KO mice are leaner and more glucose tolerant under a HFD

To determine the impact of histone variant macroH2A1 on obesity-associated increase in body weight gain, WT and macroH2A1 KO mice were fed either a chow diet or a HFD. Body weight, when being killed, in HFD-fed mice was ~10% lower in macroH2A1 KO mice compared with WT littermates ($P < 0.001$) (Figure 1a). Next, we used a DEXA analyser, an effective method in characterizing fat content and body composition, to examine the content of lean and fat masses: macroH2A1 KO displayed a significant lower amount of fat content compared with WT mice (15.58 ± 0.48 vs 17.82 ± 1.23 g, $P < 0.05$), whereas there was no statistical significant difference between the lean mass content in the groups (Figures 1b and c). In 90% of cases, human obesity is accompanied by an accumulation of lipid droplets in the hepatic parenchyma, termed NAFLD. NAFLD affects about one-third of the overall population, and it is a main risk factor for the development of non-alcoholic steatohepatitis, characterized not only by increased lipid content but also by oxidative stress, inflammation and deposition of extracellular matrix.[29] We thus sought to analyse if the lipid content in the liver of macroH2A1 KO was lower than in WT mice: surprisingly, histological analysis did not reveal evident differences between KO and WT mice, with a comparable mixed micro/macro centrolobular steatosis (Supplementary Figure S1A). Consistently, steatosis grade and NAFLD Activity Score in the centrolobular areas (zone 3 of the Rappaport's acinus) were similar in macroH2A1 KO and WT mice (Supplementary Figures S1B and C), liver TG and TC content were unaltered (Supplementary Figures S1D and E) as well as the liver weight/body weight ratios (Supplementary Figure S1F), between the two mice cohorts. Plasma levels of TGs and TCs were similar in the KO and WT mice under a HFD (Figures 1d and e). However, livers of 6 out of 15 WT mice showed increased accumulation of lymphocytes in the periportal areas (zone 1 of the Rappaport's acins), while this was absent in macroH2A1 KO mice (Supplementary Figures S2A and B), indicating the existence of periportal inflammation in WT but not in macroH2A1 KO. Circulatory glucose is kept within a tightly regulated range to provide a constant fuel supply for cell metabolism, and obesity notoriously interferes with it, often triggering the development of type 2 diabetes. Fasting plasma glucose levels were markedly reduced in KO mice upon HFD compared with WT ($P < 0.05$) (Figure 1f). A previous report described slight glucose intolerance in macroH2A1 KO male mice under a chow diet, with higher concentrations of blood glucose in intraperitoneal GTTs at all times except time point zero;[20] we were not able to reproduce these findings using an OGTT. To the contrary, upon HFD macroH2A1 KO were largely more glucose tolerant at all times tested, with larger differences observed at 90, 120 and 150 min (Figure 2a). This was reflected by a ~20% lower area under the curve (0–150 min time points) (Figure 2b). ITT showed insulin-mediated time-dependent decreases in glycaemia to a similar extent in macroH2A1 KO mice vs WT littermates (Figure 2c). To gain insight into the mechanism by which systemic glucose tolerance is maintained in HFD-fed macroH2A1 KO mice, we characterized insulin-induced AKT signaling in the skeletal muscle, liver and adipose tissues under insulin-stimulated conditions (0.75 U kg^{-1} body weight, injected 15 min before being killed) (Figures 3a and c). Interestingly, AKT phosphorylation (T308/S473) tended to be increased in the skeletal muscle tissues of macroH2A1 KO mice fed a HFD compared with WT controls (Figure 3a). This trend was absent in the liver (Figure 3b) and in the adipose tissues (Figure 3c). Altogether these findings show that the systemic absence of macroH2A1 confers mild protection from HFD-induced obesity as it protects from diet-induced weight gain. Although macroH2A1 KO are not protected against HFD-induced NAFLD, the total absence of inflammatory infiltrates in the periportal areas suggests that the presence of *macroH2A1* gene could have a proinflammatory effect in the progression of NAFLD. Regarding glucose metabolism, macroH2A1 KO mice exhibited decreased fasted glucose plasma levels and mice remained sensitive to a glucose challenge when fed an obesogenic HFD.

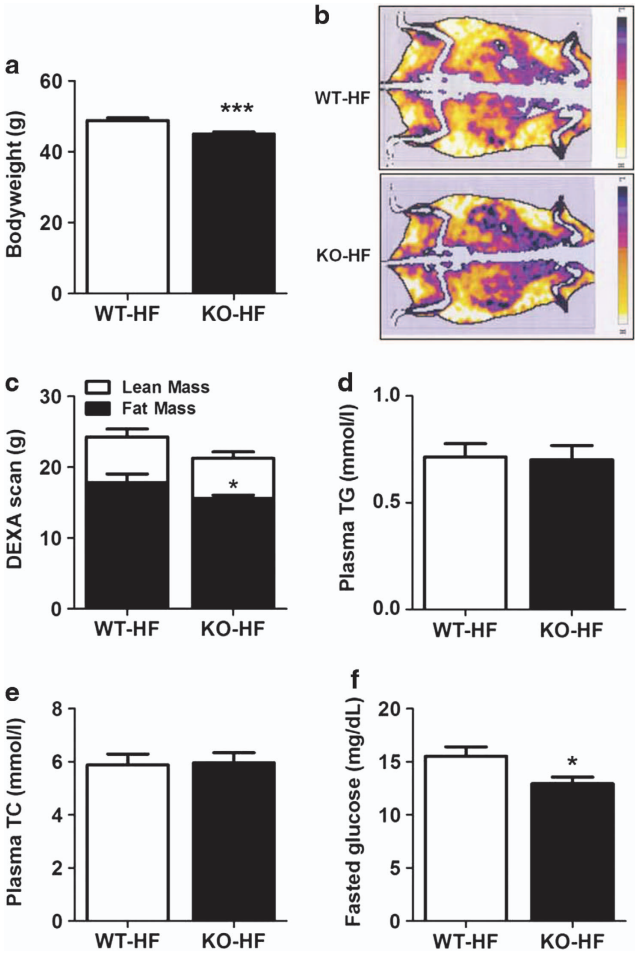

Figure 1. MacroH2A1 KO mice are protected against body weight gain and obesity after HFD. (**a**) Total body weights were measured. (**b**) Representative pictures of mice under DEXA scan. (**c**) Quantification of lean and fat mass as determined by DEXA scan analysis. (**d**) Plasma TG and (**e**) plasma TC concentrations. (**f**) Fasted glucose was measured before being killed. Values shown are means ± s.e.m. ($n = 7$–8; except body weight, $n = 14$–15). $^{*}P < 0.05$, $^{***}P < 0.001$, macroH2A1 KO vs WT.

Food intake, heat production and RER in macroH2A1 KO mice

Using metabolic cages, we ascertained if the observed difference in body weight in macroH2A1 KO mice vs WT littermates under a HFD could be because of decreased food intake and/or increased heat production. As shown in Figures 4a and c, under a standard, chow diet, macroH2A1 KO mice show a tendency towards a lower food intake and faeces production. When fed a HFD for 12 weeks,

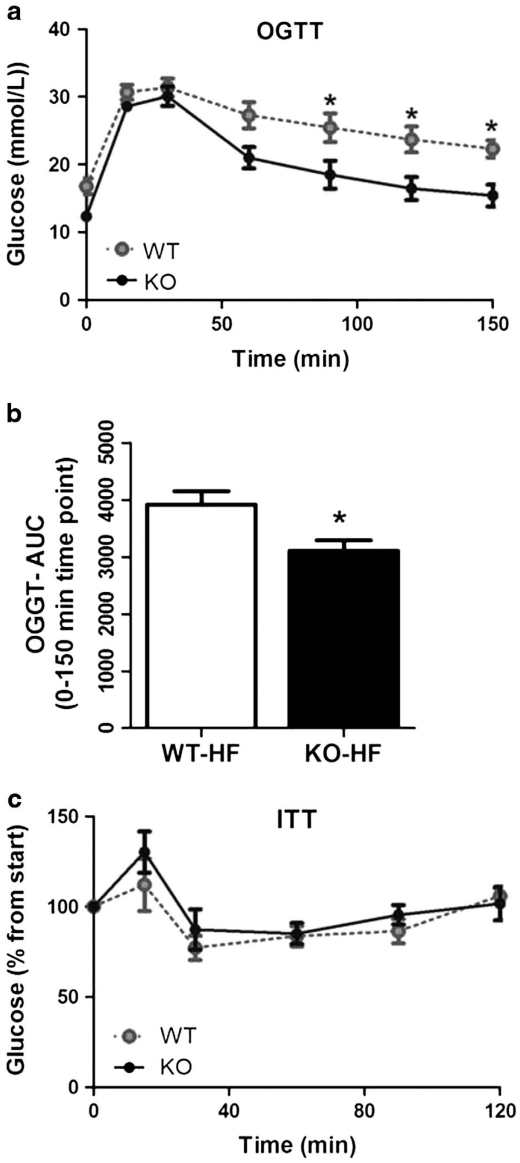

Figure 2. MacroH2A1 KO mice display increased sensitivity to glucose. (**a**) OGTT was performed in WT and macroH2A1 KO mice fed a HFD following a 6 h fast. (**b**) Area under the curve (AUC) for the OGTT. (**c**) ITT performed in WT and macroH2A1 KO mice fed a HFD following a 6 h fast. Values shown are means ± s.e.m. ($n = 7–8$). *$P < 0.05$, macroH2A1 KO vs WT.

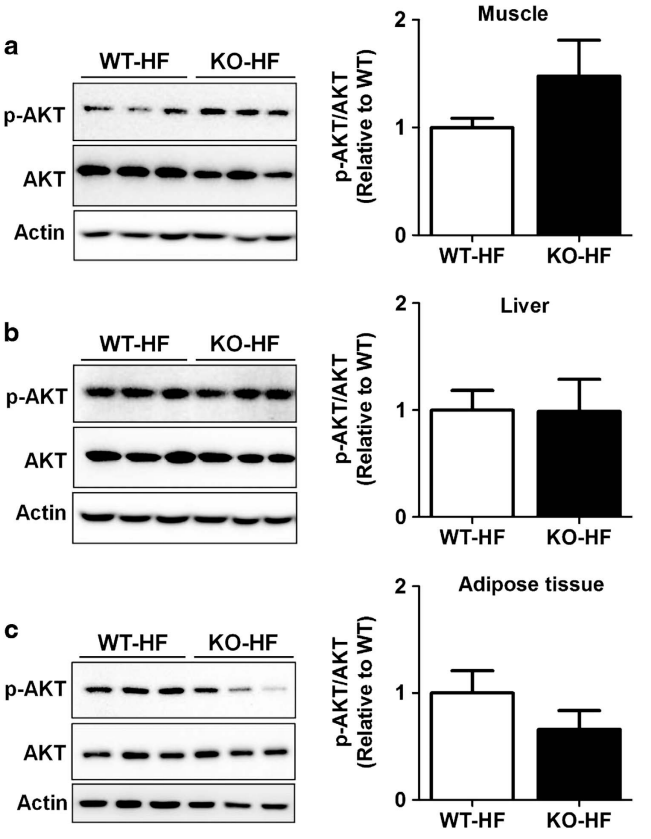

Figure 3. Increased glucose clearance is not because of enhanced insulin sensitivity in the muscle, liver and adipose tissue. Mice were injected with insulin (0.75 U kg^{-1}) 15 min before being killed, after which phosphorylation status of AKT (T308/S473) was determined by western blot. Representative immunoblots are shown in the (**a**) skeletal muscle, (**b**) liver and (**c**) adipose tissue. Immunoblots were quantified by densitometry and normalized against total protein levels of AKT. Actin was used as a loading control. Data are expressed as means ± s.e.m. ($n = 6–7$ per group). *$P < 0.05$, macroH2A1 KO vs WT.

this trend was no more evident (Figures 4b and d). Heat production was found slightly lower in macroH2A1 KO only during the day ($P < 0.05$) and under a chow diet (Figure 5a). These differences were not anymore evident upon feeding with a HFD (Figure 5b). The RER is the ratio between the amount of CO_2 produced and O_2 consumed by breathing. Measuring this ratio can be used for estimating which fuel (carbohydrate or fat) is being metabolized to supply the body with energy. RER was unaltered in macroH2A1 KO compared with WT mice regardless of the time of the day or the diet administered (chow or HFD) (data not shown). These negative data suggest that, despite some minor differences in food intake and heat production when fed a chow diet, macroH2A1 KO mice fed an obesogenic HFD diet display similar basal metabolic parameters compared with their WT littermates.

MacroH2A1 KO mice have enhanced total activity during night time under a chow diet, and during daytime under a HFD

Recent studies have pointed out the strong relationship between energy homeostasis and circadian activities at the molecular, behavioural and physiological level.[30] Experiments on rodents have shown that HFD affects total circadian activities as well as energy metabolism,[31] and alters eating behaviour. These patterns were observed because calorie intake during inactive period (daytime) increased when eating a HFD more than when eating a chow diet. Here, we measured total activity of macroH2A1 KO and WT mice under a chow diet or a HFD during daytime and night time (12 h light/12 h dark). As shown in Figure 5c, total activity was significantly increased ($P < 0.001$) in macroH2A1 KO mice under a chow diet compared with WT littermates only during night time, which is the active period. Under a HFD, macroH2A1 KO similarly displayed a slightly higher level of total activity, this time observable only during daytime, which is the inactive period. These data suggest that (i) the systemic absence of macroH2A1 might trigger epigenetically an increase in total activity and (ii) a shift in nocturnal mouse activity into daytime occurs upon a HFD feeding.

Control of genes involved in energy expenditure in BAT and VAT by macroH2A1 under a HFD

An increase in total activity is usually mirrored in an increase in energy expenditure, which might underlie the reason of the

increased leanness of macroH2A1 KO mice under a HFD. Obesity is a state of excessive accumulation of TGs in VATs because of a prolonged positive energy balance. Adipocytes are the major storage site for fat in the form of TGs. Histological analyses of visceral white adipose tissues (VAT) from macroH2A1 and WT mice fed a HFD revealed normal size and perimeter of the adipocytes on average upon quantification (Figures 6a and c), despite a decreased amount of total fat mass (Figure 1). The two types of adipose tissue, VAT and brown adipose tissue (BAT) are quite different in their location and physiological functions. VAT is the primary site of energy storage, whereas BAT is specialized for energy expenditure, and it is important for regulating body temperature: thermogenesis in BAT is fundamental to energy balance in mice and humans.[32] We sought to perform qRT-PCR gene expression studies to obtain a snapshot of the metabolic state of BAT and VAT in macroH2A1 KO mice fed an obesogenic diet. We analysed a panel of genes involved in BAT-related energy expenditure (*Ucp1* and *Fgf21*), local inflammation (interleukin-6, *Il-6*), mitochondrial oxidative capacity (*Cox4*), overall adipogenesis (*Pparγ* and *Fabp4*) and insulin-dependent glucose uptake capacity (*Glut4*). In BAT from macroH2A1 mice under a HFD, we detected a significant increase in *Ucp1*, *Glut4* and *Cox4* mRNA levels compared with WT mice (Figure 6d). These changes could be indicative of enhanced thermogenesis in BAT. In VAT the mRNA levels of the markers of adipogenesis *Pparγ*, *Glut4* and *Fabp4* were lower in the KO animals (Figure 6e), indicative of lowered adipogenic process. In conclusion, these data suggest that when fed an obesogenic HFD diet, macroH2A1 KO mice develop enhanced thermogenic gene expression in BAT and impaired proadipogenic gene expression in VAT.

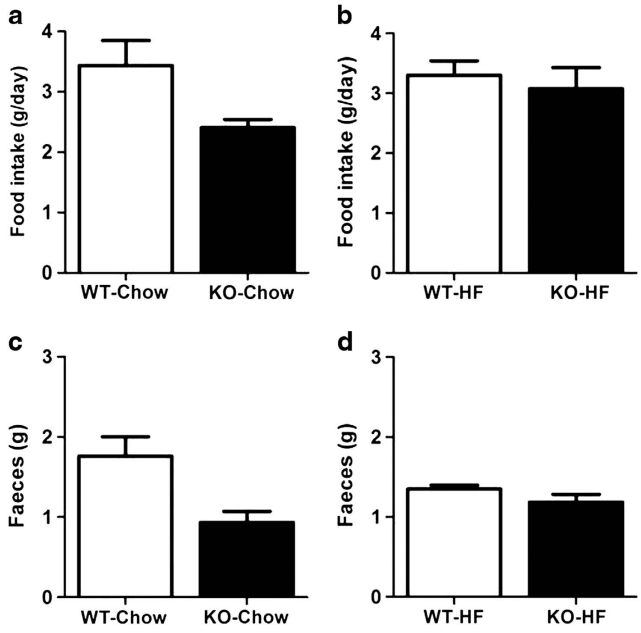

Figure 4. Food intake and faeces production are unaltered in macroH2A1 KO mice. Food intake was measured during *in vivo* metabolic analyses in mice fed a (**a**) chow diet or (**b**) a HFD. Faeces production were measured in mice fed a (**c**) chow diet or (**d**) a HFD. Values shown are means ± s.e.m. ($n = 7–8$).

DISCUSSION

MacroH2A1 is a variant of histone H2A whose transcriptional activity is implicated mechanistically *in vitro* in hepatocyte lipid accumulation, which accompanies 90% of the cases of obesity, and *in vivo* in cell stemness and tumorigenesis.[8–11,18–22] MacroH2A1 KO mice have been generated by two independent

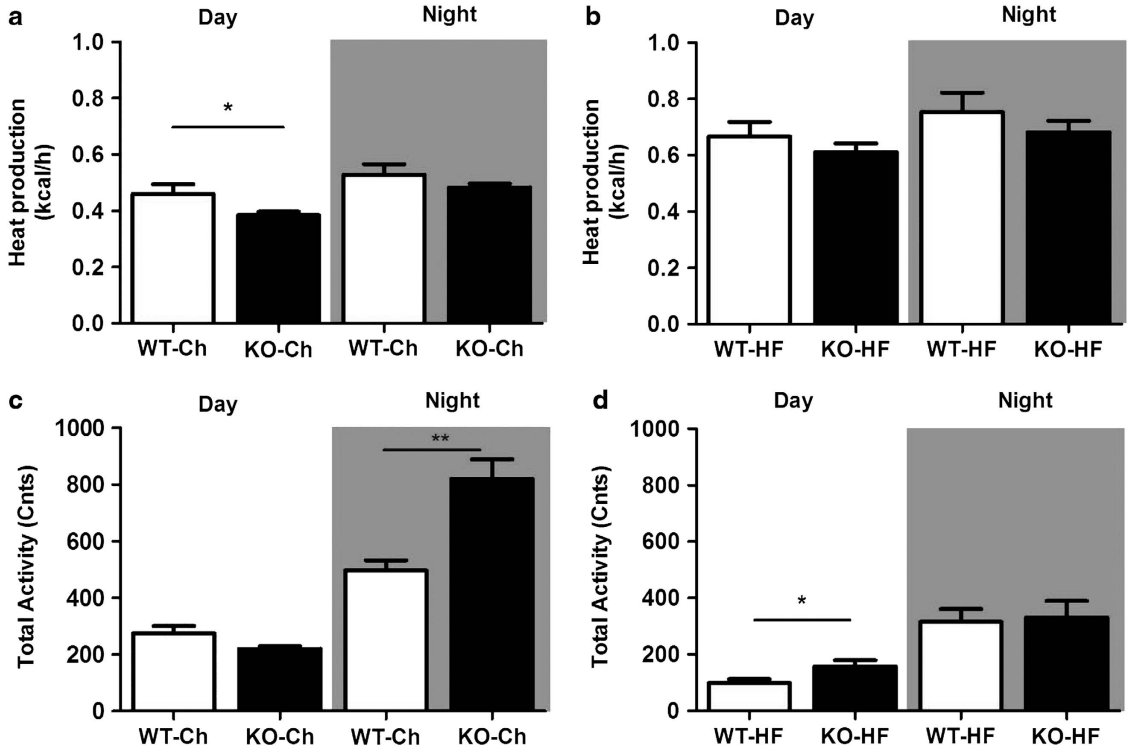

Figure 5. MacroH2A1 KO mice have lower heat production but higher total activity upon HFD feeding. Indirect calorimetric cage analysis was performed during day and night time (12-h light/12-h dark) to measure (**a**) heat production in mice fed a chow diet (**b**) and in mice fed a HFD; (**c**) total activity in mice fed a chow diet and in (**d**) mice fed a HFD. Data are expressed as means ± s.e.m. ($n = 7–8$). *$P < 0.05$, **$P < 0.01$, macroH2A1 KO vs WT.

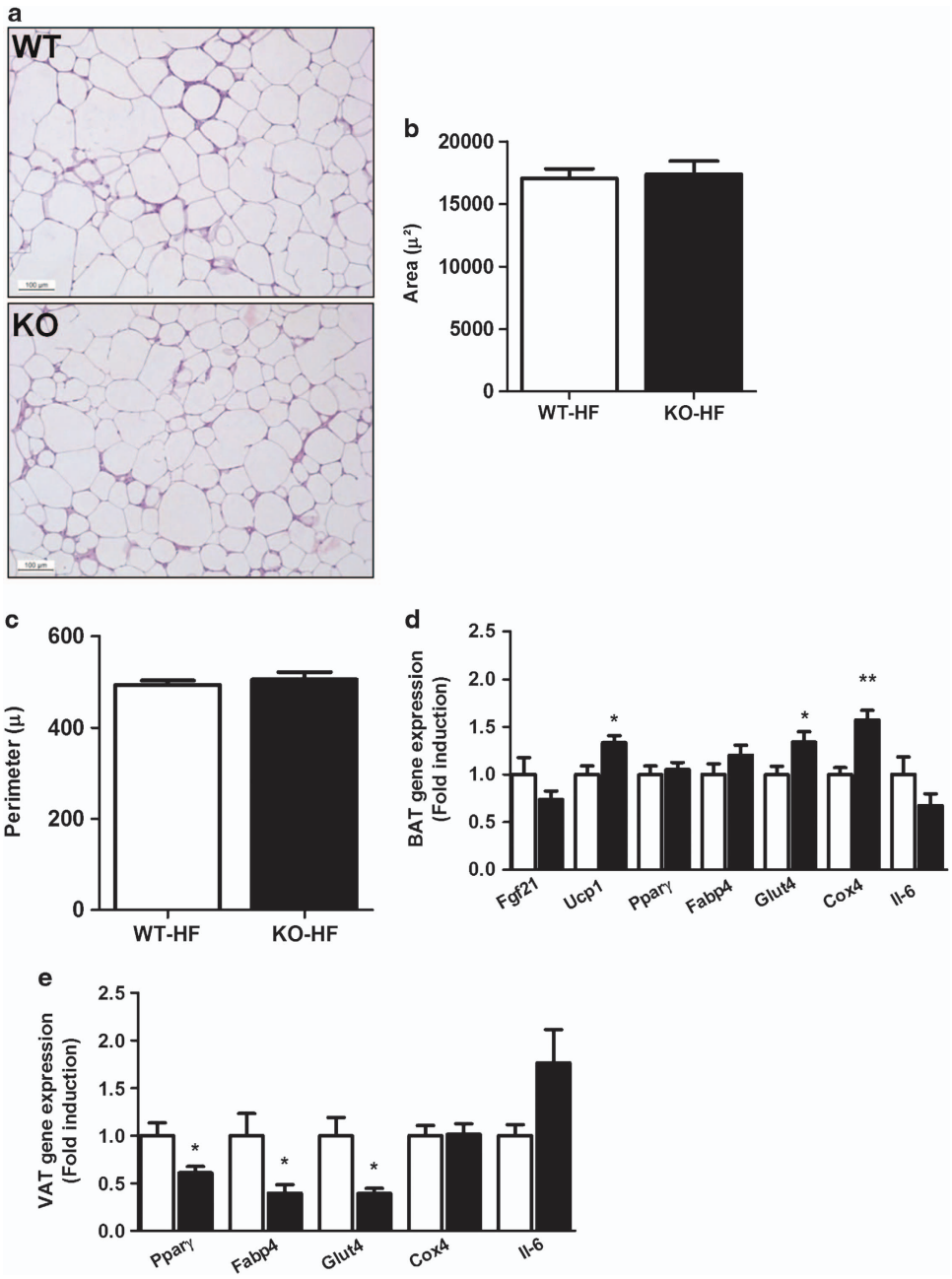

Figure 6. Increased energy expenditure-related BAT and VAT gene expression analysis in macroH2A1 KO fed a HFD. (**a**) Representative pictures from haematoxylin and eosin staining of visceral white adipose tissue (VAT) sections in WT and macroH2A1 KO mice fed with a HFD. (**b**) Quantification of VAT adipocyte area (μ^2) and (**c**) perimeter (μ) as in (**a**). (**d**) qRT-PCR analysis of mRNA expression levels of BAT *Fgf21*, *Ucp1*, *Pparγ*, *Fabp4*, *Glut4*, *Cox4* and *Il-6*. (**e**) VAT mRNA expression levels of *Pparγ*, *Fabp4, Glut4, Cox4* and *Il-6*. All mRNA expression data refer to mice fed a HFD, were normalized to the WT group and expressed as means ± s.e.m. ($n = 14$–15, except qRT-PCR, $n = 7$–8). *$P < 0.05$, ** $P < 0.01$, macroH2A1 KO vs WT.

groups and they both reported mild metabolic effects.[20,21] To understand if macroH2A1 could have systemic effects on fat accumulation and obesity, we challenged macroH2A1 KO mice with a HFD. We surprisingly found that whole-body macroH2A1 KO mice take on less fat mass than their WT littermates, without significant variations in the lean mass. Although the ablation of macroH2A1 did not alter HFD-induced lipid accumulation in comparison with WT mice, histological analysis showed periportal inflammation in 6 out of 15 of the WT mice analysed, while this was completely absent in macroH2A1 KO mice. Migration of lymphocytes towards the periportal area is very common in NAFLD spectrum.[33] During non-alcoholic steatohepatitis, periportal infiltration can then extend to the all the lobules.[34,35] Livers from HF-fed WT mice showed increased accumulation of lymphocytes around the periportal areas but not the centrolobular areas, whereas all HF-fed macroH2A1 KO mice were protected (Supplementary Figures S1 and S2). MacroH2A1 has been reported to modulate nuclear factor-κB activity in reconstituted nucleosomes,[36] and to regulate IL-8 production in B cells.[37] The mechanism by which the absence of macroH2A1 blocks the formation of inflammatory infiltrates warrants further investigation. The resistance of macroH2A1 KO mice to HFD was accompanied by decreased fasting glucose levels, an increased tolerance for glucose by OGTT and a tendency for increased

insulin sensitivity in the skeletal muscle, without enhanced insulin sensitivity in the liver or skeletal muscle. Increased glucose tolerance occurred despite the development of NAFLD in the KO mice. Although NAFLD is a strong and independent predictor for the development of type 2 diabetes, the link between insulin resistance and NAFLD has not always been demonstrated and there are a number of studies reporting dissociation of NAFLD from insulin resistance in genetic mouse models and in patients.[38–40] Our results diverge from those of Changolkar *et al.*,[20,21] reporting glucose intolerance in male mice fed a chow diet. It must be noted that we used OGTT, while this previous report used IP GTT. OGTT represents the most physiologic route of entry of glucose, and it has been shown to be more sensitive than IP GTT to detect glucose tolerance;[41] in addition, our mice were fed an obesogenic HFD diet. Moreover, a functional link between glucose intolerance and increased expression of lipogenic genes (*Lpl*, *Serpina7*, *CD36*), despite the absence of steatosis, was proposed in the liver of macroH2A1 KO mice.[20,21] This is surprising, as 80–90% of the infused glucose is uptaken by the skeletal muscle,[42] rather than the liver, consistent with the phenotype we observed in our fat model. Food intake and heat production tended to be lower in macroH2A1 KO fed a chow diet, differences that were mitigated in the presence of a HFD. Interestingly, macroH2A1 KO mice have increased total activity and display a shift in nocturnal activity into daytime upon a HFD feeding. HFD is known to affect total circadian activities as well as energy expenditure,[31] because calorie intake during inactive period increased when eating HFD. This phenotype is reminiscent of the recently proposed 'work for food' paradigm that occurs in mice when reduced food intake shifts the activity phase from night time to daytime and eventually causes nocturnal hypothermia,[43] that is, decreased heat production during night time. Whereas food restriction and HFD are extreme nutritional scenarios, we hypothesize that systemic genetic depletion of macroH2A1 might lead to adaptive flexibility in circadian organization of the behavioural timing, allowing mice to exploit the diurnal temporal niche. The functional or evolutionary advantages of these adaptive phenomena require further study, but establish a new unappreciated epigenetic link between metabolism and circadian rhythms (cycles iterating with a period of 24 ± 4 h). The biological clocks are hardwired at the cellular level by molecular oscillators working through transcriptional/translational feedback loops operated by genes and proteins fluctuating rhythmically with circadian pattern. These clocks drive the temporal variations of expression of genes encoding proteins involved in lipid and glucose metabolism (biosynthesis, transport, binding and lysis).[44,45] The expression of a huge number of these genes is influenced by the presence of macroH2A1 variants[17,20] and shows an evident circadian rhythmicity of variation, with the exception of *Apoa1*, which is characterized by ultradian rhythmicity (period < 20 h) (Supplementary Table S1). Despite the gross analysis of energy expenditure did not indicate major alterations in macroH2A1 KO mice, the assessment of gene expression in BAT revealed coordinated induction of marker genes of enhanced mitochondrial thermogenesis and glucose consumption, consistently with enhanced BAT-mediated energy expenditure in these mice. The parallel reduction in the expression of genes related to adipose accretion in VAT mirrors a scenario in which metabolic fuel is preferentially driven to energy-consuming processes (BAT) at the expense of fat deposition (VAT). The reduced fat content in KO mice would be the result of such alterations. Possibly, the mild magnitude of the process (differential accumulation of % fat in macroH2A1 KOs vs WT mice across weeks of HF diet) explains why gross measurements of energy expenditure did not allow detecting some minor, but persistent, enhancement in energy expenditure as pointed out by molecular markers in BAT. Considering that promotion of BAT-mediated energy expenditure is emerging as a potential strategy for protection against obesity and metabolic alterations (hyperglycaemia, hyperlipidaemia), current data indicate macroH2A1 inhibition as a strategy worth to explore. In this respect, functional partners of the macroH2A1 transcriptional complexes in the adipose tissue are unknown. In cancer cells, macroH2A1 recruits to the promoters of its target genes *PELP1*, a strong potentiator of retinoid X receptor activation.[46,47] In the adipose tissue, retinoid X receptor activation is crucial for reprogramming towards energy storage or thermogenesis.[48,49] Moreover, adipose tissue is at the nexus of mechanisms involved in lifespan and age-related metabolic dysfunction.[50] Obesity is associated with accelerated onset of diseases common in old age, and macroH2A1 is also a major driver in the formation of senescent-associated heterochromatin foci, one of the most prominent features of cellular senescence.[50,51] It is tempting to speculate that this epigenetic player could be at the crossroad of metabolism, energy expenditure and cellular aging.

CONFLICT OF INTEREST

The authors declare no conflict of interest.

ACKNOWLEDGEMENTS

We appreciate Dr Bastiaan Moesker, Paulina Bartuzi and Dr Marcela Aparicio-Vergara for their technical helps. FS is supported by a PhD scholarship from the Graduate School for Drug Exploration (GUIDE), University of Groningen. DPK and MHH are supported by the Center for Translational Molecular Medicine (http://www.ctmm.nl), project PREDICCt (Grant 01C-104) and by the Dutch Heart Foundation, Dutch Diabetes Research Foundation and Dutch Kidney Foundation. MV is a recipient of a My First AIRC Grant (MFAG) from Associazione Italiana per la Ricerca sul Cancro, Italy. FC is funded by Euro-Mediterranean Institute of Science and Technology, Palermo, Italy.

REFERENCES

1 Pedersen SD. Metabolic complications of obesity. *Best practice & research. Clin Endocrin Metab* 2013; **27**: 179–193.
2 Louie SM, Roberts LS, Nomura DK. Mechanisms linking obesity and cancer. *Biochim Biophys Acta* 2013; **1831**: 1499–1508.
3 Podrini C, Borghesan M, Greco A, Pazienza V, Mazzoccoli G, Vinciguerra M. Redox homeostasis and epigenetics in non-alcoholic fatty liver disease (NAFLD). *Curr Pharm Des* 2013; **19**: 2737–2746.
4 Goldberg A, Allis CD, Bernstein E. Epigenetics: a landscape takes shape. *Cell* 2007; **128**: 635–638.
5 Doye nC, An W, Angelov D, Bondarenko V, Mietton F, Studitsky VM *et al.* Mechanism of polymerase II transcription repression by the histone variant macroH2A. *Mol Cell Biol* 2006; **26**: 1156–1164.
6 Ladurner AG. Inactivating chromosomes: a macro domain that minimizes transcription. *Mol Cell* 2003; **12**: 1–3.
7 Gamble M, Frizzell KM, Yang C, Krishnakumar R, Kraus WL. The histone variant macroH2A1 marks repressed autosomal chromatin, but protects a subset of its target genes from silencing. *Genes Dev* 2010; **24**: 21–32.
8 Creppe C, Posavec M, Douet J, Buschbeck M. MacroH2A in stem cells: a story beyond gene repression. *Epigenomics* 2012; **4**: 221–227.
9 Cantarino N, Douet J, Buschbeck M. MacroH2A—an epigenetic regulator of cancer. *Cancer Lett* 2013; **336**: 247–252.
10 Barrero MJ, Sese B, Kuebler B, Bilic J, Boue S, Martí M *et al.* Macrohistone variants preserve cell identity by preventing the gain of H3K4me2 during reprogramming to pluripotency. *Cell Rep* 2013; **3**: 1005–1011.
11 Gaspar-Maia A, Qadeer ZA, Hasson D, Ratnakumar K, Leu NA, Leroy G *et al.* MacroH2A histone variants act as a barrier upon reprogramming towards pluripotency. *Nat Commun* 2013; **4**: 1565.
12 Posavec M, Timinszky G, Buschbeck M. Macro domains as metabolite sensors on chromatin. *Cell Mol Life Sci* 2013; **70**: 1509–1524.
13 Pehrson JR, Fried VA. MacroH2A, a core histone containing a large nonhistone region. *Science* 1992; **257**: 1398–1400.
14 Kustatscher G, Hothorn M, Pugieux C, Scheffzek K, Ladurner AG. Splicing regulates NAD metabolite binding to histone macroH2A. *Nat Struct Mol Biol* 2005; **12**: 624–625.
15 Ladurner AG. Rheostat control of gene expression by metabolites. *Mol Cell* 2006; **24**: 1–11.

16 Timinszky G, Till S, Hassa PO, Hothorn M, Kustatscher G, Nijmeijer B *et al.* A macrodomain-containing histone rearranges chromatin upon sensing PARP1 activation. *Nat Struct Mol Biol* 2009; **16**: 923–929.
17 Pazienza V, Borghesan M, Mazza T, Sheedfar F, Panebianco C, Williams R *et al.* SIRT1-metabolite binding histone macroH2A1.1 protects hepatocytes against lipid accumulation. *Aging* 2014; **6**: 35–47.
18 Pogribny IP, Tryndyak VP, Bagnyukova TV, Melnyk S, Montgomery B, Ross SA *et al.* Hepatic epigenetic phenotype predetermines individual susceptibility to hepatic steatosis in mice fed a lipogenic methyl-deficient diet. *J Hepatol* 2009; **51**: 176–186.
19 Rappa F, Greco A, Podrini C, Cappello F, Foti M, Bourgoin L *et al.* Immunopositivity for histone macroH2A1 isoforms marks steatosis-associated hepatocellular carcinoma. *PLoS One* 2013; **8**: e54458.
20 Changolkar LN, Costanzi C, Leu NA, Chen D, McLaughlin KJ, Pehrson JR. Developmental changes in histone macroH2A1-mediated gene regulation. *Mol Cell Biol* 2007; **27**: 2758–2764.
21 Changolkar LN, Singh G, Cui K, Berletch JB, Zhao K, Disteche CM *et al.* Genome-wide distribution of macroH2A1 histone variants in mouse liver chromatin. *Mol Cell Biol* 2010; **30**: 5473–5483.
22 Boulard M, Storck S, Cong R, Pinto R, Delage H, Bouvet P. Histone variant macroH2A1 deletion in mice causes female-specific steatosis. *Epigenet Chromatin* 2010; **3**: 8.
23 Peronnet F, Massicotte D. Table of nonprotein respiratory quotient: an update. *Can J Sport Sci* 1991; **16**: 23–29.
24 Bligh EG, Dyer WJ. A rapid method of total lipid extraction and purification. *Can J Biochem Physiol* 1959; **37**: 911–917.
25 Sheedfar F, Sung MM, Aparicio-Vergara M, Kloosterhuis NJ, Miquilena-Colina ME, Vargas-Castrillón J *et al.* Increased hepatic CD36 expression with age is associated with enhanced susceptibility to nonalcoholic fatty liver disease. *Aging (Albany NY)* 2014; **6**: 281–295.
26 Kleiner DE, Brunt EM, Van Natta M, Behling C, Contos MJ, Cummings OW *et al.* Design and validation of a histological scoring system for nonalcoholic fatty liver disease. *Hepatology* 2005; **41**: 1313–1321.
27 Salamone F, Galvano F, Cappello F, Mangiameli A, Barbagallo I, Li Volti G. Silibinin modulates lipid homeostasis and inhibits nuclear factor kappa B activation in experimental nonalcoholic steatohepatitis. *Transl Res* 2012; **159**: 477–486.
28 Planavila A, Dominguez E, Navarro M, Vinciguerra M, Iglesias R, Giralt M *et al.* Dilated cardiomyopathy and mitochondrial dysfunction in Sirt1-deficient mice: a role for Sirt1-Mef2 in adult heart. *J Mol Cell Cardiol* 2012; **53**: 521–531.
29 Pinzani M, Macias-Barragan J. Update on the pathophysiology of liver fibrosis. *Expert Rev Gastroenterol Hepatol* 2010; **4**: 459–472.
30 Bass J, Takahashi JS. Circadian integration of metabolism and energetics. *Science* 2010; **330**: 1349–1354.
31 Froy O. Circadian rhythms and obesity in mammals. *ISRN Obes* 2012; **2012**: 437198.
32 Whittle AJ, Carobbio S, Martins L, Slawik M, Hondares E, Vázquez MJ *et al.* BMP8B increases brown adipose tissue thermogenesis through both central and peripheral actions. *Cell* 2012; **149**: 871–885.
33 Bigorgne AE, Bouchet-Delbos L, Naveau S, Dagher I, Prévot S, Durand-Gasselin I *et al.* Obesity-induced lymphocyte hyperresponsiveness to chemokines: a new mechanism of fatty liver inflammation in obese mice. *Gastroenterology* 2008; **134**: 1459–1469.
34 Tilg H, Moschen AR. Evolution of inflammation in nonalcoholic fatty liver disease: the multiple parallel hits hypothesis. *Hepatology* 2010; **52**: 1836–1846.
35 Brunt EM, Kleiner DE, Wilson LA, Unalp, A, Behling, CE, Lavine, JE *et al.* Portal chronic inflammation in nonalcoholic fatty liver disease (NAFLD): a histologic marker of advanced NAFLD-Clinicopathologic correlations from the nonalcoholic steatohepatitis clinical research network. *Hepatology*, 2009; **49**: 809–820.
36 Angelov D, Molla A, Perche PY, Hans F, Côté J, Khochbin S *et al.* The histone variant macroH2A interferes with transcription factor binding and SWI/SNF nucleosome remodeling. *Mol Cell* 2003; **11**: 1033–1041.
37 Agelopoulos M, Thanos D. Epigenetic determination of a cell-specific gene expression program by ATF-2 and the histone variant macroH2A. *EMBO J* 2006; **25**: 4843–4853.
38 Aparicio-Vergara M, Hommelberg PP, Schreurs M, Gruben N, Stienstra R, Shiri-Sverdlov R *et al.* Tumor necrosis factor receptor 1 gain-of-function mutation aggravates nonalcoholic fatty liver disease but does not cause insulin resistance in a murine model. *Hepatology* 2013; **57**: 566–576.
39 Sheedfar F, Biase SD, Koonen D, Vinciguerra M. Liver diseases and aging: friends or foes? *Aging Cell* 2013; **12**: 950–954.
40 Sun Z, Lazar MA. Dissociating fatty liver and diabetes. *Trends Endocrinol Metab* 2013; **24**: 4–12.
41 Andrikopoulos S, Blair AR, Deluca N, Fam BC, Proietto J. Evaluating the glucose tolerance test in mice. *Am J Physiol Endocrinol Metab* 2008; **295**: E1323–E1332.
42 Ferrannini E, Simonson DC, Katz LD, Reichard Jr G, Bevilacqua S, Barrett EJ *et al.* The disposal of an oral glucose load in patients with non-insulin-dependent diabetes. *Metabolism* 1988; **37**: 79–85.
43 Hut RA, Pilorz V, Boerema AS, Strijkstra AM, Daan S. Working for food shifts nocturnal mouse activity into the day. *PLoS One* 2011; **6**: e17527.
44 Mazzoccoli G, Pazienza V, Vinciguerra M. Clock genes and clock-controlled genes in the regulation of metabolic rhythms. *Chronobiol Int* 2012; **29**: 227–251.
45 Mazzoccoli G, Vinciguerra M, Oben J, Tarquini R, De Cosmo S. Non-alcoholic fatty liver disease: the role of nuclear receptors and circadian rhythmicity. *Liver Int* 2014; e-pub ahead of print 20 March 2014; doi:10.111/liv.12534.
46 Singh RR, Gururaj AE, Vadlamudi RK, Kumar R. 9-*Cis*-retinoic acid up-regulates expression of transcriptional coregulator PELP1, a novel coactivator of the retinoid X receptor alpha pathway. *J Biol Chem* 2006; **281**: 15394–15404.
47 Hussey KM, Chen H, Yang C, Park E, Hah N, Erdjument-Bromage H *et al.* The histone variant macroH2A1 regulates target gene expression in part by recruiting the transcriptional coregulator PELP1. *Mol Cell Biol* 2014; **34**: 2437–2449.
48 Imai T, Jiang M, Chambon P, Metzger D. Impaired adipogenesis and lipolysis in the mouse upon selective ablation of the retinoid X receptor alpha mediated by a tamoxifen-inducible chimeric Cre recombinase (Cre-ERT2) in adipocytes. *Proc Natl Acad Sci USA* 2001; **98**: 224–228.
49 Rabelo R, Reyes C, Schifman A, Silva JE. A complex retinoic acid response element in the uncoupling protein gene defines a novel role for retinoids in thermogenesis. *Endocrinology* 1996; **137**: 3488–3496.
50 Tchkonia T, Morbeck DE, Von Zglinicki T, Van Deursen J, Lustgarten J, Scrable H *et al.* Fat tissue, aging, and cellular senescence. *Aging Cell* 2010; **9**: 667–684.
51 Zhang R, Poustovoitov MV, Ye X, Santos HA, Chen W, Daganzo SM *et al.* Formation of macroH2A-containing senescence-associated heterochromatin foci and senescence driven by ASF1a and HIRA. *Dev Cell* 2005; **8**: 19–30.

Supplementary Information accompanies this paper on International Journal of Obesity website (http://www.nature.com/ijo)